# Transition metal-modified exfoliated zirconium phosphate as an electrocatalyst for the oxygen evolution reaction

Mario V. Ramos-Garcés, <sup>1</sup> Joel Sanchez, <sup>2</sup> Daniel E. Del Toro-Pedrosa, <sup>1</sup> Isabel Barraza Alvarez, <sup>3</sup> Yanyu Wu, <sup>3</sup> Eduardo Valle, <sup>2</sup> Dino Villagrán, <sup>3</sup> Thomas F. Jaramillo, <sup>2</sup> and Jorge L. Colón <sup>1</sup>

#### **Abstract**

Improved electrochemical oxygen evolution catalysis is crucial for many clean-energy production technologies. Recently, transition metal-modified zirconium phosphate (ZrP) catalysts were studied for the oxygen evolution reaction (OER) in alkaline media. These studies suggest that the OER occurs preferentially on the surface of the layered ZrP nanoparticles rather than the interlayer gallery. Herein, ZrP nanoparticles are exfoliated with tetrabutylammonium hydroxide (TBA<sup>+</sup>OH<sup>-</sup>) to further expose surface sites which are subsequently modified with Co and Ni cations by an ion-exchange reaction. Due to the greater surface accessibility of the exfoliated ZrP support, higher loadings of catalyst material were achieved along with improved site access for catalysis. These new composite materials have improved geometric area normalized overpotentials than metal-adsorbed ZrP nanoparticles without exfoliation. Specifically, Co-modified and Ni-modified exfoliated ZrP show a reduction in overpotential at a current density of 10 mA/cm<sup>2</sup> by 41 and 181 mV, respectively.

#### Introduction

The need to satisfy the increasing global energy demand with renewable energy resources is bigger than ever. <sup>1-2</sup> For this reason, considerable research efforts have been devoted to develop technologies for clean-energy production. Technologies such as water electrolysis, electrochemical CO<sub>2</sub> reduction, metal-air batteries, and many others employ oxygen evolution as a half-cell reaction. However, the sluggish kinetics of the oxygen evolution reaction (OER), due to the transfer of four electrons and four protons, hinders the performance of these aforementioned technological devices and others, as they require high overpotentials to perform at high current densities. Hence, implementation of clean-energy production technologies at a large scale has not been possible. Designing OER catalysts with low overpotentials from earth-abundant metals while maintaining high activity and stability has been challenging. Recently, substantial progress has been made with new OER catalysts containing no noble metals that have shown promising activity and stability in alkaline conditions. <sup>5-7</sup> Nevertheless, high overpotentials are still required to turn over the reaction at the rates needed for electrocatalytic systems. <sup>8-10</sup>

One widely used strategy to improve electrocatalysts' performance is to anchor catalysts onto supports that provide synergistic electrochemical properties. For example, this strategy has yielded active catalysts for OER in recent years where it has been reported that improved conductivities and/or increased number of active sites are achievable when compared to their respective bulk systems. <sup>11-14</sup> In addition, exfoliation of layered supports has resulted in improved

<sup>&</sup>lt;sup>1</sup> Department of Chemistry, University of Puerto Rico at Río Piedras, 17 Ave. Universidad STE 1701, San Juan, PR 00925-2537, USA

<sup>&</sup>lt;sup>2</sup> Department of Chemical Engineering, Stanford University, Stanford, CA 94305, USA

<sup>&</sup>lt;sup>3</sup> Department of Chemistry and Biochemistry, University of Texas at El Paso, 500 W University Ave, El Paso, TX 79968, USA

catalysts for various reactions, including the OER, over non-exfoliated supports. The layered inorganic ion exchanger zirconium bis(monohydrogen orthophosphate) monohydrate ( $Zr(HPO_4)_2 \cdot H_2O$ ,  $\alpha$ -ZrP) has been used as a suitable intercalation nanomaterial for guest species for a wide range of applications, including, drug delivery, biosensors, artificial photosynthesis, catalysis, and others. Furthermore, studies have shown that ZrP nanoparticles can be exfoliated or their surface modified to take advantage of its cation-exchange properties to produce composite materials with greatly different properties compared to pristine ZrP.

Recently, we reported the use of ZrP as an electrocatalyst support for first-row transition metal cations for the OER.<sup>30</sup> In our study using transition metal-modified zirconium phosphate (ZrP) catalysts for the OER in alkaline media with both metal-intercalated samples and metal-adsorbed samples, we observed promising OER catalytic activity, and reported increased catalytic performance in the metal-absorbed samples over the metal-intercalated samples. These results suggest that the OER occurs preferentially on the surface of the layered ZrP nanoparticles rather than the interlayer space.<sup>30</sup> Based on these results, we expect that exposing surface sites through exfoliation of ZrP could improve these catalytic systems.

Herein, we report the preparation of exfoliated ZrP nanoparticles tetrabutylammonium hydroxide (TBA<sup>+</sup>OH<sup>-</sup>) and the modification of the exfoliated nanoparticles with divalent metals - Co and Ni. Metal-adsorbed ZrP catalysts were also prepared and characterized for performance comparisons relative to the new exfoliated composite systems. All systems underwent reaction with an excess of the metal salt precursor (10:1 metal:ZrP molar ratio), with the aim of obtaining a maximum metal loading on the systems. The new exfoliated composite materials were characterized by means of X-ray powder diffraction (XRPD), transmission electron microscopy (TEM), inductively coupled plasma spectroscopy mass spectrometry (ICP-MS), X-ray photoelectron spectroscopy (XPS), and linear sweep voltammetry (LSV). The metal-modified exfoliated ZrP particles are substantially better at adsorbing Co and Ni cations, leading to higher loadings than non-exfoliated ZrP. As such, electrochemical studies in alkaline media show that the metal-modified exfoliated ZrP nanoparticles achieve higher geometric area normalized reaction rates than the previously reported metal surface-adsorbed ZrP systems. Additionally, the performance of these catalysts are reported on turnover frequency (TOF) basis and the industrially relevant mass activity metric. Results show that the exfoliated systems maintain reasonably high intrinsic activity values that, when coupled to a significant greater number of active sites leads to higher geometric activity.

# **Experimental procedure**

#### 1.1 Materials

All chemicals were obtained from commercial sources as analytical or reagent grade and used as received. Cobalt nitrate hexahydrate (Co(NO<sub>3</sub>)<sub>2</sub>·6H<sub>2</sub>O, 98%), nickel nitrate hexahydrate (Ni(NO<sub>3</sub>)<sub>2</sub>·6H<sub>2</sub>O, 98.5%), Nafion® 117 (5% solution), zirconyl chloride octahydrate (ZrOCl<sub>2</sub>·8H<sub>2</sub>O, 98%), and tetrabutylammonium hydroxide (40% solution) were obtained from Sigma-Aldrich (St. Louis, MO, USA). Hydrochloric acid (HCl, 12.1 N), and phosphoric acid (H<sub>3</sub>PO<sub>4</sub>, 85%) were obtained from Fisher Scientific (Hampton, NH, USA). Glassy carbon rods (SIGRADUR® G, HTW Hochtemperatur-Werkstoffe GmbH, 5 mm diameter) were processed by the Stanford University crystal shop to the specifications of a 4 mm height, an area of 0.196

cm<sup>2</sup>, and the top side polished to a surface root-mean-square (RMS) roughness of less than 50 nm. Carbon black was purchased from Fuel Cell Store (College Station, TX, USA, Vulcan XC-72).

### 1.2 Synthesis

#### α-ZrP:

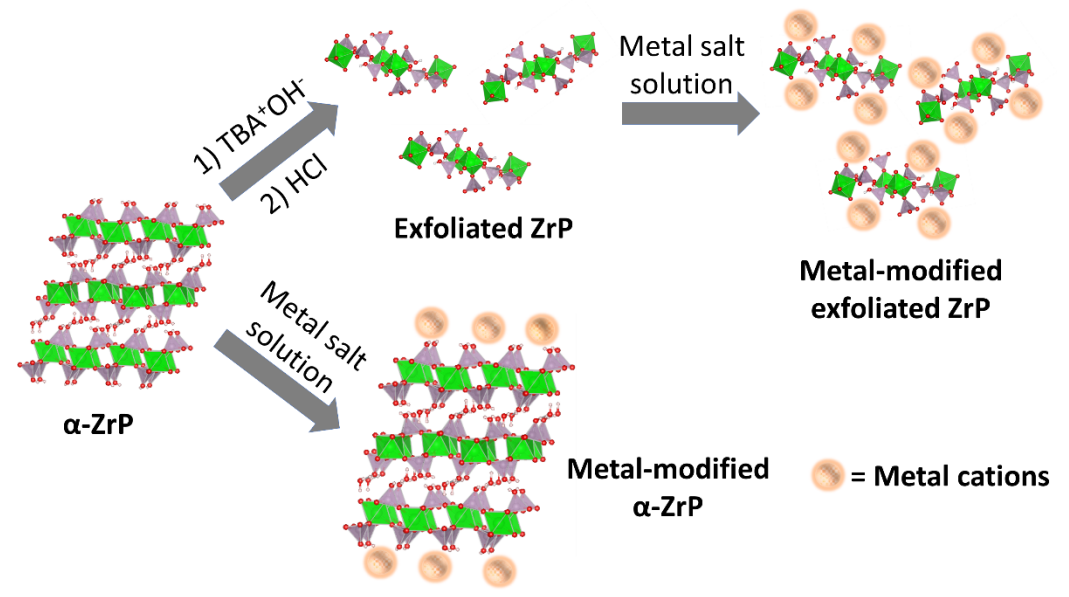
The synthesis of  $\alpha$ -ZrP was adapted from the literature.<sup>31</sup> In this procedure, 200 mL of a 0.05 M solution of ZrOCl<sub>2</sub>·H<sub>2</sub>O in deionized water was added dropwise to 200 mL of 0.05 M H<sub>3</sub>PO<sub>4</sub> solution that was pre-heated to 94 °C. This mixture was constantly stirred for 48 hours at 94 °C. The product was then filtered and washed several times with water and dried in an oven at 80 °C. Finally, the dried product was grounded into a fine powder with a mortar and pestle.

# **Exfoliated ZrP:**

To obtain the exfoliated ZrP, a modified version of the Zhou et al. procedure was used.<sup>32</sup> Exfoliation with tetra-n-butylammonium hydroxide (TBA<sup>+</sup>OH<sup>-</sup>) was performed followed by an acid treatment with HCl. First, 0.7601 g of α-ZrP was suspended in 68 mL of H<sub>2</sub>O and TBA (25.24 mL of a 0.1 M aqueous solution) was added dropwise in an ice bath. The rate of hydrolysis of ZrP during exfoliation with TBA<sup>+</sup> OH<sup>-</sup> has been found to be dependent on the temperature of the reaction and at 0 °C, hydrolysis is essentially zero.<sup>33</sup> For this reason, the exfoliation process was carried out in an ice bath to prevent ZrP hydrolysis. Second, the exfoliated ZrP (TBA<sup>+</sup>/ZrP) was protonated with an equimolar amount of HCl. This was done by adding 25.24 mL of 0.1 M HCl in dropwise fashion; the mixture was left stirring for 3 h. The protonated exfoliated ZrP was obtained by centrifugation, washing with de-ionized H<sub>2</sub>O three times to remove any residual chlorine ions.

Modification of ZrP nanoparticles and exfoliated ZrP with transition metals:

For each metal-modification, a 1 mL suspension of either the ZrP nanoparticles or exfoliated sample was prepared. To each suspension, a 1 mL solution of the intended metal



precursor salt  $(Ni(NO_3)_2 \cdot 6H_2O \text{ or } Co(NO_3)_2 \cdot 6H_2O)$  was added at a specific concentration so that the metal:ZrP molar ratio was 10:1. After mixing the metal solution with the ZrP suspensions, each reaction was left under constant stirring at room temperature for 1 day (Scheme 1). The metal- modified ZrP materials were obtained by centrifugation at 10,000 rpm for 45 mins followed by three cycles of washing with  $H_2O$ .

**Scheme 1.** Schematic representation of the metal-modification of ZrP materials.

#### 1.3 Electrochemical measurements:

#### **OER** catalytic activity:

Catalytic activity studies for the OER were performed on the metal-modified exfoliated ZrP and surface adsorbed ZrP systems. A three-electrode electrochemical cell was used in a rotating disk electrode (RDE) setup (Pine Research Instrumentation) for these measurements. OER measurements were conducted between 0.2 and 1.0 V versus the silver/silver chloride couple (Ag/AgCl) at 20 mVs<sup>-1</sup> in O<sub>2</sub>-saturated 0.1 M KOH electrolyte with an Ag/AgCl reference electrode and a platinum wire as the counter electrode. All potentials were converted and reported herein versus the reversible hydrogen electrode (RHE). The working electrode was a clean, mirror finish-polished, 5 mm diameter glassy carbon disk (GCD) modified with the metalmodified ZrP. Modification of the GCD with metal-modified exfoliated ZrP (and surface adsorbed systems) was carried out by drying a 10 µL drop of an isopropanol, carbon black, Nafion® 117 and Ni(II)- or Co(II)-modified ZrP ink (vide infra) at 600 rpm. After drying, the working electrode was composed of a thin-coating of the material supported onto the GCD. The total catalyst loading on the working electrode was of 100 µg/cm<sup>2</sup> of material, including the ZrP support. During the catalytic measurements, the working electrode was rotated at 1600 rpm. The rotation speed was fast enough to help in product removal from the surface and limit the bubble formation from oxygen evolution. Electrochemical measurements were performed on a VMP3

potentiostat/galvanostat (BioLogic Science Instruments). The solution resistance of the cell was measured at 100 kHz and *i*R-drop compensation occurred after electrochemical testing.

The intrinsic catalytic activity of both systems was determined by the TOF and the mass normalized current. Both parameters were determined at an overpotential of 0.5 V. TOFs values were calculated using the following equation:

$$TOF = \frac{J \cdot A}{4 \cdot F \cdot n}$$

Where J is the current density at 1.73 V versus RHE, A is the surface area of the GCD (0.196 cm<sup>2</sup>), F is the Faraday constant (96,485.3329 s·A·mol<sup>-1</sup>), and n is the number of moles of either Co or Ni on the electrode. As a conservative estimate of the TOF we assume that all metal atoms are electrochemically active and participating in the OER.

#### Ink preparation for GDC modification:

Each catalyst ink was prepared by dispersing 2.5 mg of carbon black and 5 mg of the metal modified-ZrP system into 2.55 mL of isopropanol and 10.02 μL of Nafion® 117. Carbon black was added to increase conductivity. The ink was sonicated until it was well dispersed.

## 2.4 Physical and chemical characterization (XRPD, ICP-MS, TEM, XPS):

To elucidate whether ZrP was successfully exfoliated, XRPD data was obtained using a Rigaku (Tokyo, Japan) SuperNova single crystal X-ray diffractometer in micro diffraction mode with Cu  $K_{\alpha}$  radiation ( $\lambda = 1.5417$ Å) equipped with a HyPix3000 X-ray detector in transmission mode operated at 50 kV and 1 mA. Measurements were collected at 300 K from 6 to 40° (in the  $2\theta$  axis) with a step of  $0.01^{\circ}$  using the Gandolfi move experiment for powders. The d spacing was calculated using Bragg's law ( $n\lambda = 2d_{hkl}\sin \theta$ ), where  $\lambda$  is the wavelength of the X-ray source,  $d_{hkl}$  is the interlayer distance between planes in the unit cell, and  $\theta$  is the diffraction angle. Quantitative determination of the cobalt and nickel loading of our samples was done by Inductively Coupled Plasma Mass Spectrometry (ICP-MS) measurements. All samples were digested in an aqua-regia matrix overnight and were diluted and filtered to a 5% acid concentration by volume for analysis. Samples were analyzed in a Thermo Scientific (Waltham, MA, USA) XSeries 2 ICP-MS and all standard solutions (Ni and Co) were TraceCERT® certified and obtained from Sigma-Aldrich. The morphology of the ZrP nanoparticles and exfoliated ZrP was studied by transmission electron microscopy (TEM) using a FEI Tecnai (Thermo Fisher Scientific, Inc.) microscope operated at 200 kV. The chemical state and atomic ratio of P/Zr for α-ZrP and exfoliated ZrP were examined using high resolution XPS (PHI 5000 VersaProbe, Physical Electronics, Enzo, Chigasaki, Japan) with an Al Kα source. All spectra were calibrated to the adventitious carbon 1s peak at 284.8 eV and fitted using a Shirley background. Atomic concentrations were calculated using the relative peak area ratio of the Zr 3d peak and the P 2p peak.

#### **II.** Results and Discussions

#### Physical and chemical characterization (XRPD, TEM, XPS)

Figure 1 shows the XRPD patterns of  $\alpha$ -ZrP, exfoliated ZrP and the metal-modified exfoliated ZrP materials. The synthesis of  $\alpha$ -ZrP nanoparticles resulted in a crystalline material

as evidenced by the XRPD pattern (Figure 1). The diffraction peak at  $2\theta = 11.6^{\circ}$  corresponds to an interlayer distance of 7.6 Å which correlates to the characteristic interlayer spacing of  $\alpha$ -ZrP. In addition, the (020) and (31 $\overline{2}$ ) reflections at ca. 34° are present, which indicate  $\alpha$ -like layer arrangement. Exfoliation of  $\alpha$ -ZrP was carried out by intercalation of TBA<sup>+</sup> ions in a high molar ratio to form a TBA<sup>+</sup> double layer in the interlayer space, leading to exfoliation due to cation-cation repulsions. The exfoliated surface was then protonated by an acid wash of HCl to regenerate the hydroxyl groups of the phosphate groups. The successful displacement of TBA<sup>+</sup> ions by H<sup>+</sup> was monitored by the absence of a characteristic diffraction peak at ca. 15.4 Å attributed to restacked TBA<sup>+</sup>/ZrP. After protonation, the diffraction patterns of the exfoliated systems show the extreme broadening characteristic of successful ZrP exfoliation. Similar diffractograms are observed for the metal modified exfoliated ZrP confirming that no further restacking occurs after metal modification.

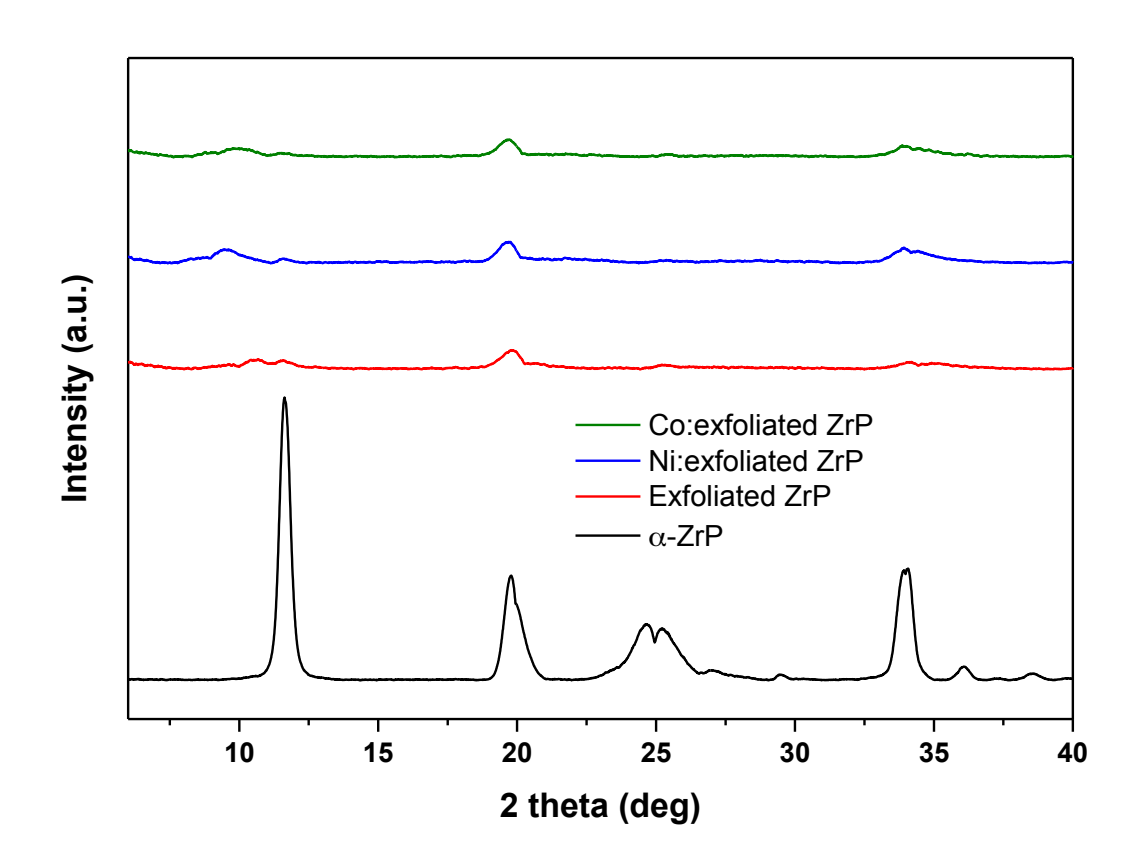


**Figure 1.** XRPD patterns of  $\alpha$ -ZrP, exfoliated ZrP, and metal-modified exfoliated ZrP samples.

Transmission electron microscopy (TEM) micrographs of the  $\alpha$ -ZrP nanoparticles show their characteristic hexagonal shape (Figure 2a and 2b). Our nanoparticles, synthetized by the reflux method of Kijima, have diameters of ca. 150 nm. The exfoliated ZrP was also characterized by TEM. After the exfoliation procedure, the exfoliated ZrP retains its hexagonal morphology and has a diameter of ca. 150 nm. No hydrated zirconia nanoparticles are observed decorating the edges of the sheets, indicating that the hydrolysis prone edges were preserved by temperature control during the exfoliation reaction and that the structure of the layers did not

change.<sup>33</sup> When compared to the  $\alpha$ -ZrP micrographs, the exfoliated ZrP shows a fainter contrast which is consistent with its thinner nature, since in TEM areas that contain heavy atoms or are thick appear darker.<sup>15</sup>

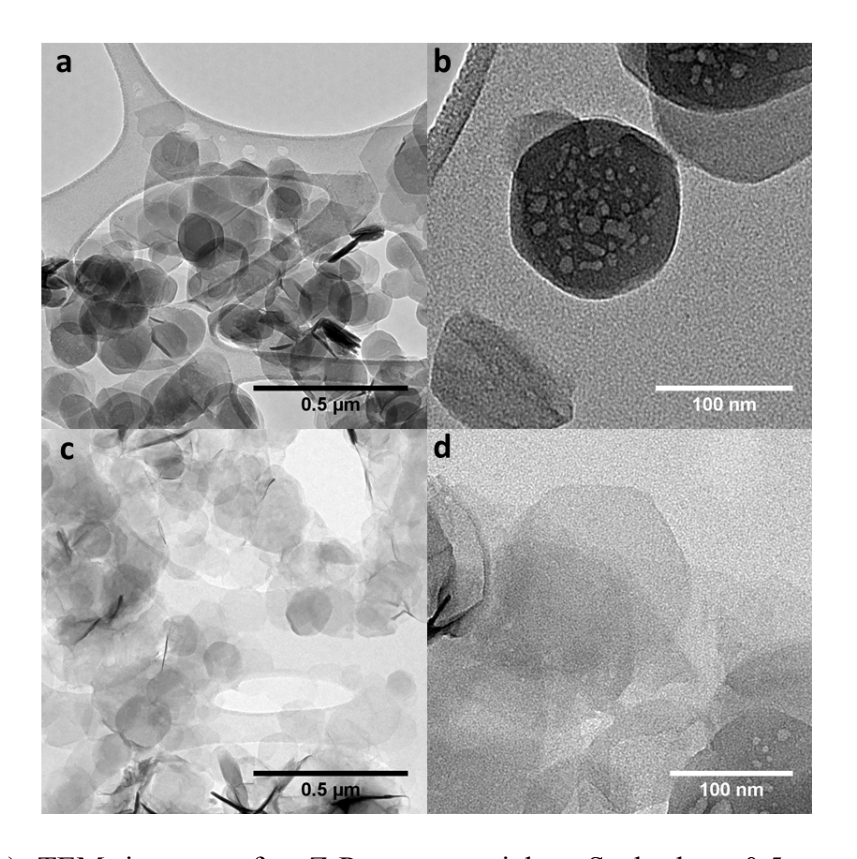


**Figure 2.** (a-b) TEM images of  $\alpha$ -ZrP nanopareticles. Scale bar, 0.5  $\mu$ m and 100 nm, respectively. (c-d) TEM images of exfoliated ZrP. Scale bar, 0.5  $\mu$ m and 100 nm, respectively.

X-ray photoelectron spectroscopy (XPS) was performed to further elucidate if any chemical changes occurred after the successful TBA<sup>+</sup> exfoliation of  $\alpha$ -ZrP. Figure 3a indicates that pristine  $\alpha$ -ZrP and exfoliated ZrP show similar survey spectral lines and high-resolution (Figure 3b and 3c) Zr 3d and P 2p scans show that no drastic chemical shifts were observed. Additionally, the P/Zr ratio stays consistent at ~2 indicating that corrosion from producing insoluble ZrO<sub>2</sub> and soluble phosphate did not occur before and after TBA<sup>+</sup> exfoliation.<sup>38</sup>

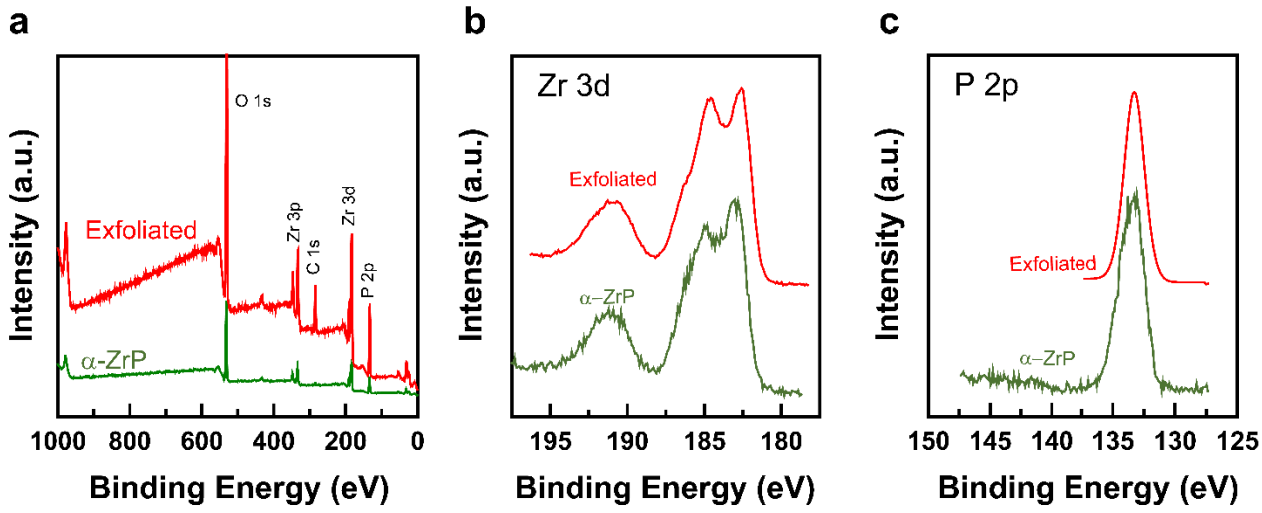


**Figure 3.** (a) XPS spectra of  $\alpha$ -ZrP and exfoliated ZrP. (b-c) High-resolution XPS scans of Zr 3d and 2p signals.

#### **Electrochemical measurements**

The metal-modified exfoliated ZrP catalysts were tested for their activity towards the OER in 0.1 M KOH electrolyte. Cyclic voltammetry was used to assess the activity for these systems, as well as for the metal-modified surface adsorbed ZrP materials. The metrics used to measure OER activity were the overpotential at  $10 \text{ mA/cm}^2$  ( $\eta_{10}$ ) and  $3 \text{ mA/cm}^2$  ( $\eta_3$ ) and the Tafel slope. The overpotential measured at  $10 \text{ mA/cm}^2$  is the potential difference between the potential to achieve  $10 \text{ mA/cm}^2$  and the thermodynamic potential of water oxidation (1.23 V vs RHE). However, for the nickel samples, we report the overpotential at a current density of  $3 \text{ mA/cm}^2$  so we can do a direct comparison since the surface adsorbed system did not reach  $10 \text{ mA/cm}^2$  at the applied potential range.

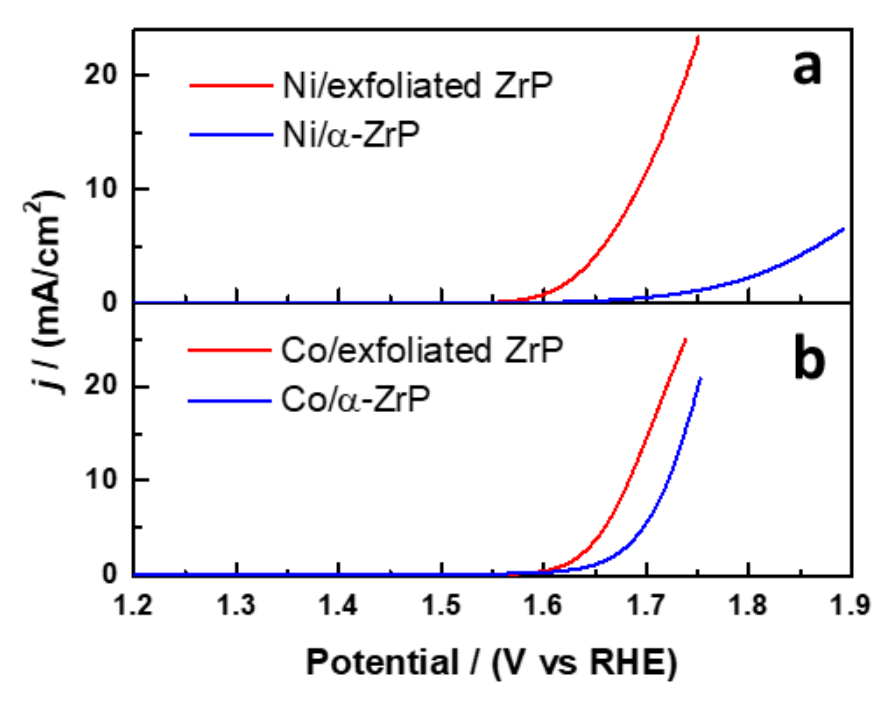


**Figure 4.** Linear sweep voltammograms of (a) Ni(II)/ZrP systems, and (b) Co(II)/ZrP systems.

Figure 4a shows the linear sweep voltammograms (LSVs) of Ni/exfoliated ZrP and surface adsorbed Ni/ZrP and Figure 4b shows the LSV of Co/exfoliated ZrP and surface adsorbed Co/ZrP. In both exfoliated cases, the potentials for the observed OER currents were shifted to lower values when compared to the surface adsorbed systems. Specifically, the overpotential for the Co/exfoliated ZrP material is 0.450 V, while for the Co/ZrP is 0.491 V. For the Ni/exfoliated ZrP and Ni/ZrP materials, the overpotential is 0.410 V and 0.592 V, respectively.

Figure 5a and 5b show the Tafel plots for the Ni(II) and Co(II) systems, respectively. The higher catalytic activity of the exfoliated systems is also reflected in their lower-angled Tafel slopes. This means that the exfoliated samples require less additional overpotential to increase their catalytic currents. The values of the Tafel slopes are summarized in Table 1. Specifically, Tafel slopes for Ni/ZrP and Ni/exfoliated ZrP are 131.9 and 55.1 mVdec<sup>-1</sup>, respectively; while for Co/ZrP and Co/exfoliated ZrP are 79.0 and 53.4 mVdec<sup>-1</sup>, respectively. The improved Tafel slopes after exfoliation could indicate a number of possibilities: improved kinetics, mass transport, and or electron transport. Similar effects have been observed in other studies. <sup>15,39</sup>

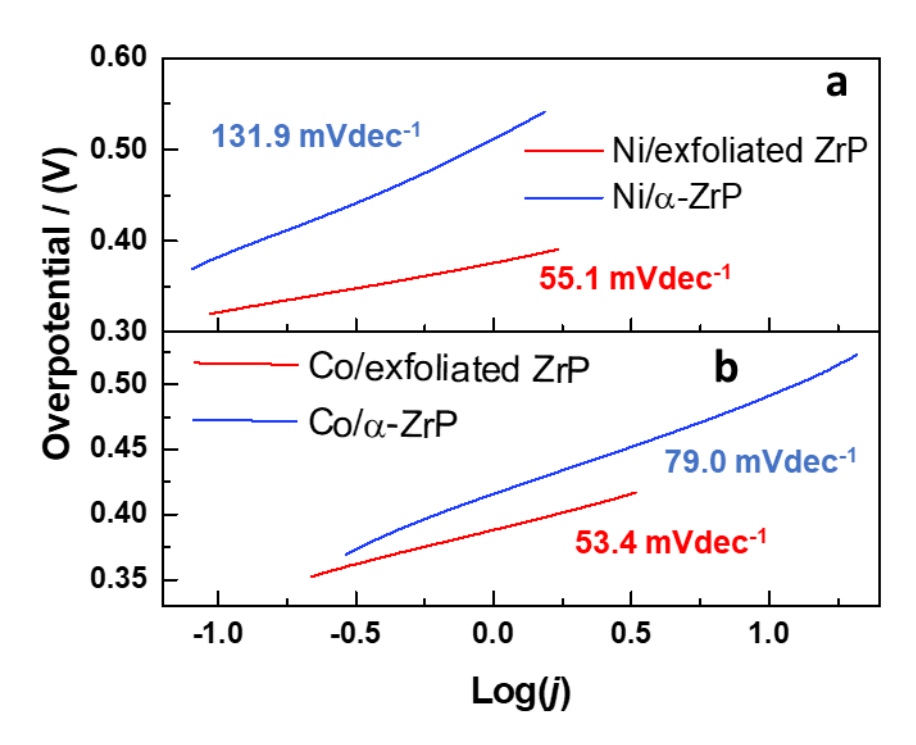


**Figure 5.** Tafel plots of (a) Ni(II)/ZrP systems, and (b) Co(II)/ZrP systems.

To further characterize the nature of the increased activity, we calculated the intrinsic activity of each catalytic site in both types of systems. The metrics used to determine the intrinsic activity were the turnover frequency and the mass normalized current. For this, we performed ICP-MS measurements on our samples to quantify the amount of nickel and cobalt metal content in the exfoliated and bulk materials. In our calculations, we assumed that all metal content quantified by ICP-MS in the materials were active and accessible to perform OER. While this

method represents the lower limit of the true TOF values, it enables a consistent comparison for both types of systems.<sup>7</sup>

Figure 6a and 6b show the LSVs where the catalytic currents were normalized by the mass of the metal content. The TOF and mass normalized activity values for each catalyst are presented in Table 1. For the Ni(II) systems the mass normalized current for the exfoliated material stays relatively the same as for the bulk counterpart at all overpotentials. In addition, at an overpotential of 0.5 V the TOF values remain similar for the Ni/exfoliated ZrP and Ni/ZrP (0.09 s<sup>-1</sup> and 0.10 s<sup>-1</sup>, respectively). For the Co(II) systems, Figure 6b shows that the mass normalized current remains relatively the same except at higher overpotentials; at an overpotential of 0.5 V, the mass normalized current for the bulk system is twice of that of the exfoliated material. Similarly, the TOF values for the Co/exfoliated ZrP and Co/ZrP are 0.48 s<sup>-1</sup> and 1.04 s<sup>-1</sup>, respectively.

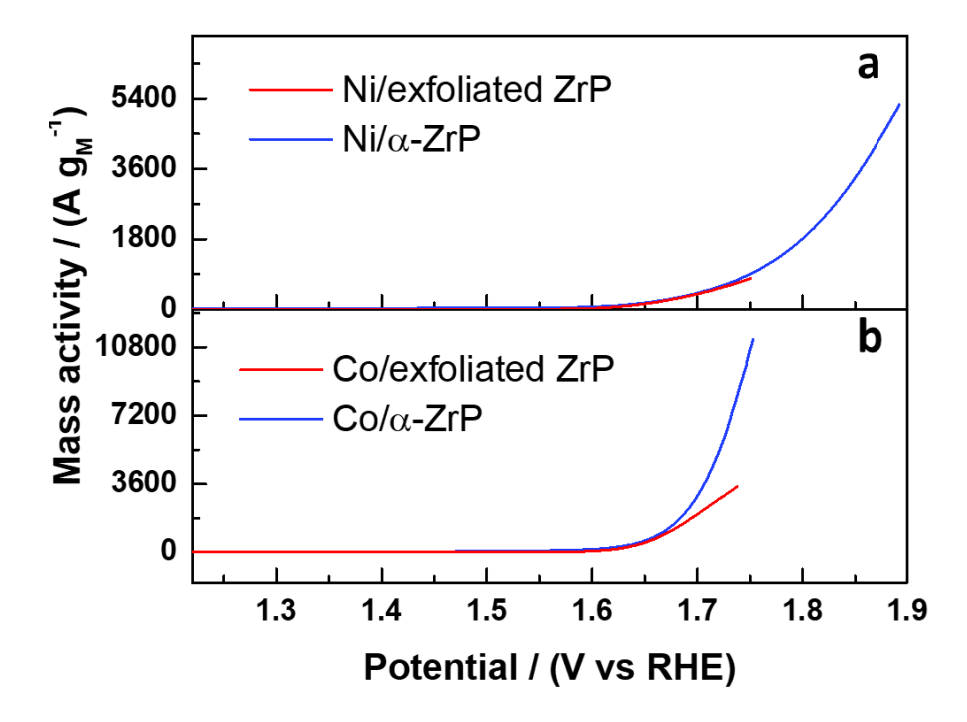


**Figure 6.** Mass normalized catalytic currents for (a) Ni(II)/ZrP systems, and (b) Co(II)/ZrP systems.

**Table 1.** Metal mass percent and selected performance electrochemical values for the metal-modified ZrP catalysts.

Catalyst	Metal percent (%)	η <sub>10</sub> or η <sub>3</sub> (V)	Tafel slope (mV/dec)	Mass activity @ $\eta = 0.5 \text{ V (A/g}_{\text{M}})$	$TOF @  \eta = 0.5 V  (s-1)$
Ni(II):α- ZrP adsorbed	$1.251 \pm 0.009$	0.592	131.9	684	0.10
Ni(II):α- ZrP exfoliated	$29.33 \pm 4.32$	0.410	55.1	610	0.09
Co(II):α-ZrP adsorbed	$1.855 \pm 0.009$	0.491	79.0	6814	1.04
Co(II):α-ZrP exfoliated	$7.21 \pm 1.40$	0.450	53.4	3147	0.48

These results show that the increased activity of the exfoliated samples is not due to higher intrinsic activity of the catalytic sites. Instead, the enhanced OER performance can be attributed to a larger number of active sites as observed by the higher metal content determined by ICP-MS. On this note, the drastically improved activity for the nickel system can be explained by the much higher metal exchange capacity that the exfoliated ZrP presents for this metal, which is around 23 times higher than the bulk ZrP. Previous studies have shown that ZrP systems where metals are intercalated have less activity for OER than the ones where the metals are surface-adsorbed, even when there is a higher metal content on those systems.<sup>30</sup> For this reason we believe that the enhancement in catalytic activity is due to the fact that the inner layer surfaces are now more electrochemically accessible stemming from being more exposed to the electrolyte in the exfoliated samples.

#### III. Conclusions

Our results indicate that metal exchange on exfoliated ZrP leads to better OER performance in alkaline media than metal exchange with layered ZrP nanoparticles. The metal-modified exfoliated ZrP particles are substantially better at adsorbing Co and Ni cations, leading to higher loadings than non-exfoliated ZrP. These systems maintain reasonably high intrinsic activity values that, when coupled to a significant greater number of active sites leads to higher geometric activity. In addition, this enhanced activity is shown in the lower-angled Tafel slopes for both exfoliated materials studied herein. This work paves the way for future investigations of ZrP as support for active catalytic materials.

#### **Corresponding authors**

\*(J.L.C.) E-mail: jorge.colon10@upr.edu \*(T.F.J.) E-mail: jaramillo@stanford.edu

#### Notes

The authors declare no competing financial interest.

## **Acknowledgements:**

This work was supported by the National Science Foundation under the NSF Center for Chemical Innovation in Solar Fuels CHE-1305124. Part of this work was performed at the Stanford Nano Shared Facilities (SNSF), supported by the National Science Foundation under award ECCS- 1542152. The single crystal X-ray diffractometer was acquired through the support of the National Science Foundation under the major instrumentation award number CHE-1626103. MVRG was supported by the National Science Foundation under the NSF Center for Chemical Innovation in Solar Fuels CHE-1305124 and the NSF-PREM Center for Interfacial Electrochemistry of Energy Materials (CiE2M) grant DMR-1827622. JS was supported by the Department of Defense (DoD) through the National Defense Science and Engineering Graduate Fellowship (NDSEG) Program and Stanford University Diversifying Academia, Recruiting Excellence Doctoral Fellowship Program (DARE). DEDTP was supported by the NSF sponsored Puerto Rico-Louis Stoke Alliance for Minority Participation at UPR-RP, award number 1400868. IBA was supported by the Undergraduate Biomedical Research Training at UTEP/MARC, grant

number 2T34GM008048, and by the Summer Research – Early Identification Program (SR-EIP) at Stanford University. We would also like to acknowledge the Molecular Sciences Research Center of the University of Puerto Rico.

#### References:

- 1) Lewis, N.S.; Nocera, D.G. Powering the planet: Chemical challenges in solar energy utilization. *Proc. Natl. Acad. Sci.* **2006**, *103*, 15729-15735.
- 2) Gray, H. B. Powering the planet with solar fuel. *Nature Chem.* **2009**, *1*, 7.
- 3) Montoya, J.H.; Seitz, L.C.; Chakthranont, P.; Vojvodic, A.; Jaramillo, T.F.; Nørskov, J.K. Materials for solar fuels and chemicals. *Nat. Mater.* **2016,** *16*, 70-81.
- 4) Jiao, Y.; Zheng, Y.; Jaroniec, M.; Qiao, S.Z. Design of electrocatalysts for oxygen- and hydrogen-involving energy conversion reactions. *Chem. Soc. Rev.* **2015**, *44*, 2060-2086.
- 5) Cheng, Y.; Jiang, S. P. Advances in electrocatalysts for oxygen evolution reaction of water electrolysis-from metal oxides to carbon nanotubes. *Prog. Nat. Sci.* **2015**, *25*, 545-553.
- 6) Hunter, B. M.; Gray, H. B.; Müller, A. M. Earth-abundant heterogeneous water oxidation catalysts. *Chem. Rev.* **2016**, *116*, 14120-14136.
- 7) Song, F.; Bai, L.; Moysiadou, A.; Lee, S.; Hu, C.; Liardet, L.; Hu, X. Transition metal oxides as electrocatalysts for the oxygen evolution reaction in alkaline solutions: An application-inspired renaissance. *J. Am. Chem. Soc.* **2018**, *140*, 7748-7759.
- 8) McCrory, C.C.L.; Jung, S.; Peters, J.C.; Jaramillo, T.F. Benchmarking heterogeneous electrocatalysts for the oxygen evolution reaction. *J. Am. Chem. Soc.* **2013**, *135*, 16977-16987.
- 9) McCrory, C.C.L.; Jung, S.; Ferrer, I.M.; Chatman, S.M.; Peters, J.C.; Jaramillo, T.F. Benchmarking hydrogen evolving and oxygen evolving electrocatalysts for solar water splitting devices. *J. Am. Chem. Soc.* **2015**, *137*, 4347-4357.
- 10) Jung, S.; McCrory, C.C.L.; Ferrer, I.M.; Peters, J.C.; Jaramillo, T.F. Benchmarking nanoparticulate metal oxide electrocatalysts for the alkaline water oxidation. *J. Mater. Chem. A.* **2016**, *4*, 3068-3076.
- 11) Gong, M.; Li, y.; Wang, H.; Liang, Y.; Wu, J.Z.; Zhou, J.; Wang, J.; Regier, T.; Wei, F.; Dai, H. An advanced Ni-Fe layered double hydroxide electrocatalyst for water oxidation. *J. Am. Chem. Soc.* **2013**, *135*, 8452-8455.
- 12) Wu, J.; Liu, Y.; Geng, D.; Liu, H.; Meng, X. Cobalt oxide nanosheets anchored onto nitrogen-doped carbon nanotubes as dual purpose electrodes for lithium-ion batteries and oxygen evolution reaction. *Int. J. Energy Res.* **2017**, *42*, 853-862.
- 13) Zhao, S.; Rasimick, B.; Mustain, W.; Xu, H. Highly durable and active Co<sub>3</sub>O<sub>4</sub> nanocrystals supported on carbon nanotubes as bifunctional electrocatalysts in alkaline media. *Appl. Catal. B* **2017**, 138-145.
- 14) Ding, Y.; Klyushin, A.; Huang, X.; Jones, T.; Teschner, D.; Girgsdies, F.; Rodenas, T.; Schlögl, R.; Heumann, S. Cobalt bridged with ionic liquid polymer on carbon nanotube for enhanced oxygen evolution reaction activity. *Angew. Chem. Int. Ed.* **2018**, *57*, 3514-3518.
- 15) Song, F.; Hu, X. Exfoliation of layered double hydroxides for enhanced oxygen evolution catalysis. *Nat. Commun.* **2014,** *5,* 4477.
- 16) Liang, H.; Meng, F.; Cabán-Acevedo, M.; Li, L.; Forticaux, A.; Xiu, L.; Wang, Z.; Jin, S. Hydrothermal continuous flow synthesis and exfoliation of NiCo layered double

- hydroxide nanosheets for enhanced oxygen evolution catalysis. *Nano Lett.* **2015**, *15*, 1421-1427.
- 17) McAteer, D.; Godwin, I.J.; Ling, Z.; Harvey, A.; He, L.; Boland, C.S.; Vega-Mayoral, V.; Szydlowska, B.; Rovetta, A.A.; Backes, C.; Boland, J.B.; Chen, X.; Lyons, M.E.G.; Coleman, J.N. Liquid exfoliated Co(OH)<sub>2</sub> nanosheets as low-cost, yet high-performance, catalysts for the oxygen evolution reaction. *Adv. Energy Mater.* **2018**, *8*, 1702965.
- 18) Xiao, H.; Liu, S. Zirconium phosphate (ZrP)-based functional materials: Synthesis, properties and applications. *Mater. Des.* **2018**, *155*, 19-35.
- 19) Díaz, A.; González, M.L.; Pérez, R.J.; David, A.; Mukherjee, A.; Báez, A.; Clearfield, A.; Colón, J.L. Direct intercalation of cisplatin into zirconium phosphate nanoplatelets for potential cancer nanotherapy. *Nanoscale* **2013**, *5*, 11456-11463.
- 20) González-Villegas, J.; Kan, Y.; Bakhmutov, V.I.; García-Vargas, A.; Martínez, M.; Clearfield, A.; Colón, J.L. Poly(ethylene glycol)-modified zirconium phosphate nanoplatelets for improved doxorubicin delivery. *Inorg. Chim. Acta* **2017**, *468*, 270-279.
- 21) Feng, J.-J; Xu, J.-J.; Chen, H.-Y. Synergistic effect of zirconium phosphate and Au nanoparticles on direct electron transfer of hemoglobin on glassy carbon. *J. Electroanal. Chem.* **2005**, *585*, 44-50.
- 22) Santiago, M.B.; Vélez, M.M.; Borrero, S.; Díaz, A.; Casillas, C.A.; Hofmann, C.; Guadalupe, A.R.; Colón, J.L. NADH electrooxidation using bis(1,10-phenantroline-5,6-dione)(2,2'-bipyridine)ruthenium(II)-exchanged zirconium phosphate modified carbon paste electrode. *Electroanalysis* **2006**, *18*, 559-572.
- 23) Atienzar, P.; Victoria-Rodríguez, M.; Juanes, O.; Rodríguez-Ubis, J.C.; Brunet, E.; García, H. Layered γ-zirconium phosphate as novel semiconductor for dye-sensitized solar cells: Improvement of photovoltaic efficiency by intercalation of a ruthenium complex-viologen dyad. *Energy Environ. Sci.* **2011**, *4*, 4718-4726.
- 24) Pica, M. Zirconium phosphate catalysts in the XXI century: State of the art from 2010 to date. *Catalysts* **2017**, *7*, 190.
- 25) Zhou, Y.; Noshadi, I.; Ding, H.; Liu, J.; Parnas, R.S.; Clearfield, A.; Xiao, M.; Meng, Y.; Sun, L. Solid acid catalyst based on single-layer α-zirconium phosphate nanosheets for biodiesel production via esterification. *Catalysts* **2018**, *8*, 17.
- 26) Rosati, O.; Lanari, D.; Scavo, R.; Persia, D.; Marmottini, F.; Nocchetti, M.; Curini, M.; Piermatti, O. Zirconium potassium phosphate methyl and/or phenyl phosphonates as heterogeneous catalysts for Knoevenagel condensation under solvent free conditions. *Microporous Mesoporous Mater.* **2018**, *268*, 251-259.
- 27) Pica, M.; Donnadio, A.; Casciola, M. From microcrystalline to nanosized α-zirconium phosphate: Synthetic approaches and applications of an old material with a bright future. *Coord. Chem. Rev.* **2018**, *374*, 218-235.
- 28) Troup, J.M.; Clearfield, A. On mechanism of ion exchange in zirconium phosphates. 20. Refinement of the crystal structure of α-zirconium phosphate. *Inorg. Chem.* **1977**, *16*, 3311–3314.
- 29) Alberti, G.; Casciola, M.; Costantino, U.; Vivani, R. Layered and pillared metal(IV) phosphates and phosphonates. *Adv. Mater.* **1996,** *8*, 291-303.
- 30) Sanchez, J.; Ramos-Garcés, M.V.; Narkeviciute, I.; Colón, J.L.; Jaramillo, T.F. Transition metal-modified zirconium phosphate electrocatalysts for the oxygen evolution reaction. *Catalysts* **2017**, *7*, 132.

- 31) Kijima, T. Direct preparation of  $\theta$ -zirconium phosphate. *Bull. Chem. Soc. Jpn.* **1982,** 55, 3031-3032.
- 32) Zhou, Y.; Huang, R.; Ding, F.; Brittain, A.D.; Liu, J.; Zhang, M.; Xiao, M.; Meng, Y.; Sun, L. Sulfonic acid-functionalized α-zirconium phosphate single-layer nanosheets as a strong solid acid for heterogeneous catalysis applications. *ACS Appl. Mater. Interfaces* **2014**, *6*, 7417-7425.
- 33) Kaschak, D.M.; Johnson, S.A.; Hooks, D.E.; Kim, H.-N.; Ward, M.D.; Mallouk, T.E. Chemistry on the edge: A microscopic analysis of the intercalation, exfoliation, edge functionalization, and monolayer surface tiling reactions of α-zirconium phosphate. *J. Am. Chem. Soc.* **1998**, *120*, 10887-10894.
- 34) Alberti, G. Syntheses, crystalline-structure, and ion-exchange properties of insoluble acid salts of tetravalent metals and their salt forms. *Acc. Chem. Res.* **1978**, *11*, 163–170.
- 35) Sun, L.; Boo, W. J.; Sue, H.-J.; Clearfield, A. Preparation of alpha-zirconium phosphate nanoplatelets with wide variations in aspect ratios. *New J. Chem.* **2007**, *31*, 39–43.
- 36) Díaz, A.; Saxena, V.; González, J.; David, A.; Casañas, B.; Batteas, J.; Colón, J.L.; Clearfield, A.; Hussain, M. Zirconium phosphate nano-platelets: a platform for drug delivery in cancer therapy. *Chem. Commun.* **2012**, *48*, 1754-1756.
- 37) Sun, L.; Boo, W.J.; Sun, D.; Clearfield, A.; Sue, H.-J. Preparation of exfoliated epoxy/α-zirconium phosphate nanocomposites containing high aspect ratio nanoplatelets. *Chem. Mater.* **2007**, *19*, 1749-1754.
- 38) Kim, H.-N.; Keller, S.W.; Mallouk, T.E. Characterization of zirconium phosphate/polycation thin films grown by sequential adsorption reactions. *Chem. Mater.* **1997,** *9*, 1414-1421.
- 39) Vrubel, H.; Moehl, T.; Grätzel, M.; Hu, X. Revealing and accelerating slow electron transport in amorphous molybdenum sulphide particles for hydrogen evolution reaction. *Chem. Commun.* **2013**, *49*, 8985-8987.